Metabolic Topology of Neurodegenerative Disorders: Influence of Cognitive and Motor Deficits

Oliver Granert[1], Alexander E. Drzezga[2], Henning Boecker[3], Robert Perneczky[4–6], Alexander Kurz[6], Julia Götz[1], Thilo van Eimeren[1], and Peter Häussermann[7,8]

[1]Department of Neurology, Kiel University, Kiel, Germany; [2]Department of Nuclear Medicine, University of Cologne, Cologne, Germany; [3]Department of Radiology, Bonn University, Bonn, Germany; [4]Neuroepidemiology and Ageing Research Unit, Imperial College of Science, Technology and Medicine, London, United Kingdom; [5]Cognitive Impairment and Dementia Services, West London Mental Health NHS Trust, London, United Kingdom; [6]Department of Psychiatry, TU Munich, Munich, Germany; [7]Department of Psychiatry, Kiel University, Kiel, Germany; and [8]LVR Clinic Cologne, Academic Teaching Hospital, University of Cologne, Cologne, Germany

Parkinson disease with and without dementia (PDD and PD, respectively), dementia with Lewy bodies (DLB), and Alzheimer dementia (AD) traditionally have been viewed as distinct clinical and pathologic entities. However, intriguing overlaps in biochemical, clinical, and imaging findings question the concept of distinct entities and suggest a continuous spectrum in which individual patients express PD-typical patterns and AD-typical patterns to a variable degree. **Methods:** Following this concept, we built a topological map based on regional patterns of the cerebral metabolic rate of glucose as measured with ^{18}F-FDG PET to rank and localize single subjects' disease status according to PD-typical (PD vs. controls) and AD-typical (AD vs. controls) pattern expression in patients clinically characterized as PD, PDD, DLB, amnestic mild cognitive impairment, and AD. **Results:** The topology generally confirmed an indivisible spectrum of disease manifestation according to 2 separable expression patterns. The expression values derived from the first pattern were highly correlated with individual cognitive, but not motor, disability. The opposite was found for the corresponding expression values of the second pattern. **Conclusion:** The metabolic imaging analysis supports the notion that there is a continuous spectrum of neurodegeneration between AD and PD. Furthermore, PDD and DLB may in fact represent 1 overlapping disease entity, characterized by the presence of mixed neuropathology and only different by the time course.

Key Words: Alzheimer; Parkinson; FDG PET; dementia; motor deficits

Age-related neuropsychiatric disorders such as Parkinson disease with and without dementia (PDD and PD, respectively), dementia with Lewy bodies (DLB), amnestic mild cognitive impairment (aMCI), and Alzheimer disease dementia (AD) represent a growing socioeconomic challenge. However, these disorders show substantial clinical and neuropathologic overlap, limiting diagnostic accuracy and questioning the concept of distinct clinical entities (*1–3*). Indeed, the notion that PD and AD may be extremes of a spectrum of neurodegenerative diseases—with DLB and PDD presenting overlapping neuropathologic and clinical features within this spectrum—has received growing attention in recent years (*4*).

Although pathophysiologically and clinically different, PD and AD share some aspects in common: both are age-related neurodegenerative disorders characterized by aggregation of pathologic proteins leading to dysfunction of cerebral networks and distinct patterns of metabolic changes (*3–6*). Cases characterized by pure PD (α-synuclein aggregation) or pure AD (amyloid and tau aggregation) pathology do not represent most affected patients. Biologically and histopathologically, there is an overlap of these age-associated proteinopathies. They form a continuum with concomitant amyloid-, tau-, and α-synuclein aggregation as well as microvascular changes (*6,7*).

aMCI represents an intermediate clinical state of cognitive decline between normal aging and AD, showing histopathologic and neurobiochemical similarities to AD (*8,9*). DLB and PDD are also age-related neurodegenerative disorders sharing clinical and histopathologic aspects with both PD and AD (*7,10*). Hence, they can be seen as intermediate neurodegenerative disorders in a spectrum between pure PD and pure AD. Because the pattern of histopathology, neuronal network dysfunction, and associated clinical deficits is indeed continuous, the traditional view of distinct disease entities is increasingly being questioned.

A biomarker-based approach targeted to disentangle histopathology–clinical relationships within this spectrum may further help to guide classification of neurodegenerative disorders and treatment stratification. ^{18}F-FDG is an established imaging biomarker of neurodegeneration. In AD, characteristic deficits of the regional cerebral metabolic rate of glucose (rCMRglc) involve temporoparietal and posterior cingulate cortices (*11*). ^{18}F-FDG uptake in PD is most consistently characterized by metabolic changes within frontotemporal and parietooccipital areas (*12–14*).

In this study, we aimed to explore the spectrum of the most common age-related neurodegenerative disorders, ranging from PD to AD on a metabolic level. In contrast to previous studies on this topic, using pairwise group comparisons of different disease groups, we were especially interested in the analysis of different disease groups in relation to the parkinsonian and dementia-related marginal patterns (AD and PD vs. controls). Our goal was to metabolically explore the full neurodegenerative spectrum

(PD-PDD-DLB-aMCI-AD) and depict it in 1 common topological map.

MATERIALS AND METHODS

Participants

The analysis was based on a cohort of 100 patients with aMCI, 91 patients with AD, 20 patients with PD, 17 patients with PDD, and 26 patients with DLB as compared with 24 elderly controls (CON). All subjects underwent whole-brain ^{18}F-FDG PET under resting conditions. Structural imaging (CT or MR) was performed in all participants to exclude structural abnormalities of the brain beyond cortical atrophy.

Patients with aMCI/AD were recruited from a university memory clinic, whereas patients with PD, PDD, and DLB were recruited from a university movement disorder clinic. Patients with AD met National Institute of Neurological and Communicative Disorders and Stroke/ Alzheimer's Disease and Related Disorders Association criteria for probable AD (15). None of the patients with AD or aMCI showed parkinsonian symptoms. All patients were seen both by a movement disorder specialist and by a psychiatrist from the memory clinic. Diagnosis of PD was made by consensus between experienced clinicians using the U.K. Brain Bank criteria for PD (16). The severity of parkinsonian motor symptoms was rated using the unified Parkinson's disease rating scale (UPDRS) III motor scale (17). Dementia in PD was diagnosed according to the *Diagnostic and Statistical Manual of Mental Disorders* (DSM-IV) and consensus criteria for PDD (10,18). DLB was diagnosed according to McKeith (18), whereas aMCI was diagnosed according to the International Working Group on MCI criteria (19). Neuropsychologic evaluation was based on the battery of the Consortium to Establish a Registry for Alzheimer disease scores (20).

Differences in the clinical and neuropsychologic findings were assessed between groups using the nonparametric Mann–Whitney U test or χ^2 test. Results are given as mean value and corresponding SD. P values are 2-tailed, and significance level was set at a value of less than 0.05.

In accordance with the Declaration of Helsinki, the experimental procedures were explained, and a written informed consent form was signed by all subjects and, where appropriate, by their caregivers. The study had the approval of the local ethics committee and radiation protection authorities.

PET

Each patient fasted for at least 6 h before PET scanning. Dopaminergic and cholinergic medication was transiently stopped at least 12 h before scanning. PET images were acquired in 3-dimensional mode using a Siemens ECAT EXACT HR+ scanner (CTI). Intravenous injection of 185 MBq of ^{18}F-FDG was performed with subjects at rest (eyes closed, dimmed ambient light, no movement). A 20-min static acquisition protocol beginning 30 min after injection was used. Transmission scans were obtained for attenuation-correction purposes using a rotating [68]Ge/^{68}Ga source. After corrections for randoms, dead time, and scatter, images were reconstructed with filtered backprojection (Hamm filter, cutoff frequency, 0.5 cycles/projection element) resulting in 60–63 slices in a 128 × 128 matrix (pixel size, 2 mm) and interplane separation of 2.4 mm.

Preprocessing and Analysis of Imaging Data

The PET image data were preprocessed and analyzed with the SPM8 software (Wellcome Department of Cognitive Neurology) and MATLAB 7.11.0.584 (The MathWorks Inc.). Stereotactic normalization was performed using the SPM8 default PET template. The normalization resulted in a standardized image set in the Montreal Neurologic Institute space. The normalized images were smoothed with an isotropic gaussian filter (12 mm in full width at half maximum). Radioactivity distribution was analyzed semiquantitatively by normalizing regional cerebral ^{18}F-FDG PET use by linear proportional scaling to a default value of 50 mL/dL/min.

For statistical analysis, the preprocessed datasets were compared voxel by voxel between the marginal subgroups (AD and PD) of patients and the control group (CON) using 2-sample t tests, assuming unequal variances between the groups. To evaluate the spatial distribution of the metabolic differences between our marginal groups (AD, PD, CON), we calculated statistical t maps for all possible group comparisons. For visualization purposes, in Figure 1 and Supplemental Figure 1 (supplemental materials are available at http://jnm.snmjournals.org), the statistical threshold was set to a uncorrected P value of less than 0.001 for all contrasts of interest (AD vs. CON, PD vs. CON, and AD vs. PD) to show the full extent of metabolic differences.

All groupwise comparisons were visually inspected and compared with previous findings. However, detailed results of the statistical analyses are not reported here. We refer all interested readers to the study of Teune et al. (14), in which equivalent groups were systematically tested against a control group using a similar image processing procedure with comparable results.

Pattern Analysis

Disease-specific expression values of voxel-based spatial covariance patterns were determined using the t map projection method (21). This approach is closely related to a method described by Worsley et al. (22), assessing the global significance of pattern differences.

Mathematically, the projection method corresponds to the scalar product of 2 vectors, in which the vectors are the concatenated intensity values of the voxels in the normalized and smoothed PET images (first vector) and the SPM t maps (second vector). The resulting scalar
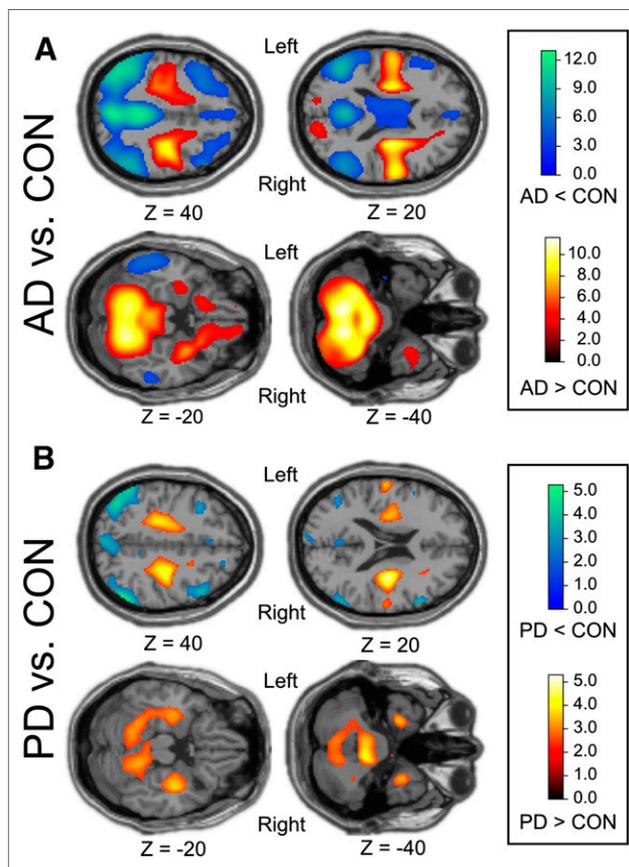
FIGURE 1. Statistical maps used to calculate expression values. (A) T-contrast AD versus CON. (B) T-contrast PD versus CON. Statistical maps were shown with threshold of uncorrected P value < 0.001 and overlaid onto single subject T1 template.

(individual expression value) is used as 1 coefficient for the expression vector. To remove voxels with less discriminative power, we additionally applied a threshold of $|T| \geq 2$ to the statistical maps. Using the t maps of the contrasts AD-CON and PD-CON to project subject-specific metabolic patterns gave 2-dimensional expression vectors representing the manifestation of the disease-specific rCMRglc pattern for each subject. The first dimension represents the Alzheimerlike metabolic pattern, whereas the second corresponds to the Parkinsonlike metabolic pattern. Decorrelation of the 2 expression scores was realized by a principal component (PC)–based whitening transformation. The resulting new whitened feature space represents our metabolic topological map. To access the informative value of these new features, we analyzed the feature space in 3 different ways:

First, we estimated these new features for all our subjects in all groups (AD, PD, PDD, DLB, aMCI, and CON). The corresponding features were plotted into the 2-dimensional topographic feature space (Fig. 2) for visual presentation of the feature distribution. Second, we evaluated the 2 dimensions of our new remapped (decorrelated) feature vectors for correlations with the most important clinical features in our setting (cognitive deficits, that is, Mini Mental State Examination [MMSE] scores, and extrapyramidal motor disturbances, that is, UPDRS III scores). The correlations were tested with nonparametric Spearman correlation tests (Fig. 3).

Finally, a groupwise analysis was performed by a Kruskal–Wallis χ^2 test, followed by Wilcoxon post hoc tests to access statistically relevant differences of the topological features between groups. All statistical tests were performed using an α-level P value of less than 0.05.

RESULTS

Clinical Data

Demographic and clinical variables are displayed in Tables 1 and 2. All groups have similar age ranges (mean age in groups, 68–71 y) except for the group of aMCI patients, which was slightly
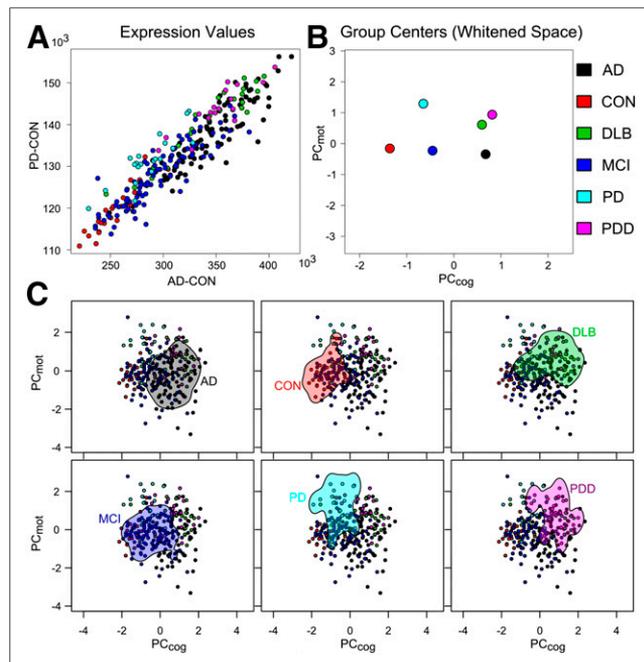
FIGURE 2. Metabolic topological map. (A) Statistical maps used to calculate expression values correspond to group t-contrasts: AD < CON and PD < CON. (B) Positions of group means in normalized/whitened PC space. (C) Distribution in overall normalized feature space (aligned and scaled along 2 PCs, PC_{cog} and PC_{mot}) with colored area inside isocurve of constant feature density for each of our patient groups.
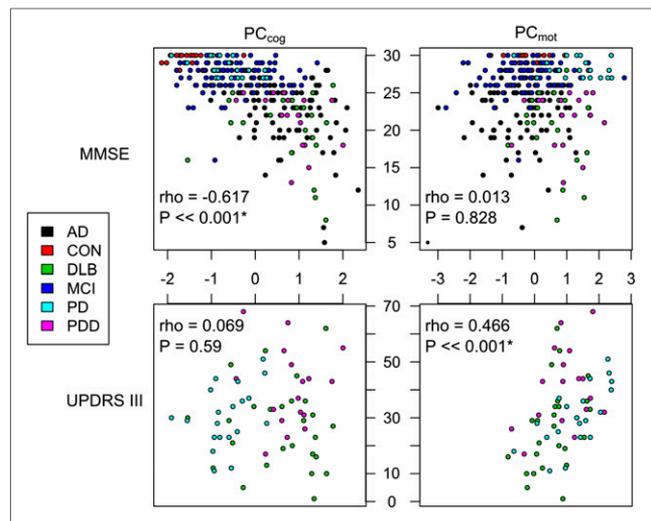
FIGURE 3. Correlation between PCs and clinical scores. Projections to PCs have strong negative correlation with MMSE (PC_{cog}) and strong positive correlation with motor UPDRS III scale (PC_{mot}). Decomposition/whitening according to PC of original datasets allows differentiation of clinical symptoms cognitive deficits and motor deficits based on their metabolic patterns.

younger (mean age, 65 y). The MMSE scores can be divided into 3 partitions. The first partition is the nondemented partition (CON, PD), the second partition is represented by the groups with a strong cognitive impairment (AD, DLB, PDD), and the third partition with the aMCI group lies between the 2 other partitions and shows significantly different MMSE values as compared with the other groups. The UPDRS III scores were available only for the groups with motor deficits (DLB, PD, and PDD). The motor deficits were comparable in the DLB and PD groups, whereas the patients with PDD had significantly higher UPDRS III scores than patients with PD and DLB.

Metabolic Pattern Comparisons Between Marginal Groups

The voxelwise SPM group comparisons with the CON group and the 2 marginal groups (PD and AD) exhibited typical and distinct metabolic profiles for both the PD and the AD groups (Fig. 1). The Alzheimer group (AD vs. CON) showed a decline of rCMRglc bilaterally in the posterior cingulate cortex, the lateral temporal lobe (Brodmann area 20/21) and the inferior parietal cortex. Temporoparietal and posterior cingulate reductions of rCMRglc in the group of AD patients is in accordance with previous imaging studies (Fig. 1A) (14,23–26). The group of patients with PD (PD vs. CON) exhibited frontal and parietooccipital hypometabolism as well as temporal and pontocerebellar hypermetabolism (Figs. 1B and 4B). This pattern is closely related to a previous neuroimaging study using proportionally scaled datasets (14).

Finally, we compared the groups DLB and PDD using 2-sample t tests and found no metabolic differences between these groups either on peak or on cluster level ($P < 0.05$, familywise error corrected).

Calculation and Evaluation of Topological Features

Projection of the individual rCMRglc maps onto these disease-specific patterns provided 2 expression values for the subjects of all groups, showing a high correlation (Fig. 2A). Transformation by a decorrelation mapping (whitening transform) to a principal component (PC)–aligned coordinate frame revealed the meaningful patterns in the feature space (Figs. 2B and 2C). The first PC (labeled

TABLE 1
Group Demographics

Group	n	Sex (M/F)	Mean age	Mean MMSE	Mean UPDRS III
AD	91	46/45	69.47 (7.78)	22.51 (4.25)	—
CON	24	12/12	69.92 (6.30)	29.38 (0.82)	0.3 (0.68)*
DLB	26	14/12	71.73 (6.50)	21.54 (5.34)	26.77 (15.01)
MCI	100	51/49	65.79 (9.06)	27.18 (2.00)	—
PD	20	14/6	67.65 (9.27)	28.25 (1.21)	30.65 (10.93)
PDD	17	14/3	70.76 (7.34)	21.41 (3.71)	40.71 (14.23)

*Only $n = 10$ UPDRS III measurements were available for CON group.
Data in parentheses are SDs.

PC_{cog} according to the correlation with cognition-related MMSE score) captures most of the variance of the original projection data, whereas the second PC (labeled PC_{mot} according to the correlation with motor-related UPDRS III) captures the orthogonal variance.

To validate the expression values, we tested for correlations with clinical scores. The first dimension (PC_{cog}) of the features vectors showed high correlation with the MMSE score ($\rho = -0.617$; $P \ll 0.001$) and no relation to the motor-related UPDRS III score ($\rho = 0.013$; $P = 0.828$), whereas the second dimension (PC_{mot}) showed no correlation with the dementia score MMSE ($\rho = 0.069$; $P = 0.59$) but strong correlation with the UPDRS III score ($\rho = 0.466$; $P \ll 0.001$). A summary of the results of the correlation analysis is presented in Figure 3.

A further support of the informative value gave the groupwise comparisons. Here the expression values showed a significant group effect (Kruskal–Wallis χ^2: PC_{cog} leads to $\chi^2 = 136.5$, degrees of freedom $= 5$, $P \ll 0.001$; PC_{mot} leads to $\chi^2 = 72.5$, degrees of freedom $= 5$, $P \ll 0.001$), and the post hoc tests revealed the domain-specific differences of the 2 feature dimensions. The detailed results of the post hoc tests with the 2 components are given in Table 2.

The decorrelated features correspond to a decoupling of dementia (PC_{cog})- and motor (PC_{mot})-related symptoms. However, the metabolic patterns of these decorrelated features are also of interest and can deviate from the patterns of the original group comparisons. Therefore, we reconstructed the spatial metabolic patterns on the basis of the whitening transform determined in the feature space. This reconstruction corresponds to a weighted recombination of the original AD versus CON and PD versus CON patterns according to the whitening transform and is visualized in Figure 4.

DISCUSSION

We built a topological map based on rCMRglc patterns measured with ^{18}F-FDG PET. The map resampled a topology corresponding to clinical categorization and therefore can be used to rank and localize patients within this metabolic map (Figs. 2B and 2C). The Parkinson-related pattern and the dementia-related pattern are determined by metabolic changes, which are important predictors of the individual disease status and the extent of neurodegeneration (Fig. 4).

The construction of this topological map is solely based on the 2 contrast patterns derived from the AD < CON and PD < CON comparisons, with no statistical correction for clinical scores or severity of symptoms. However, the topological features PC_{cog} and PC_{mot}, representing each patient's position on the metabolic map, were clearly influenced by the severity of cognitive and motor deficits as shown by our correlation analysis (Fig. 3).

TABLE 2
Metabolic and Clinical Group Comparisons

	AD MMSE	AD UPDRS III	MCI MMSE	MCI UPDRS III	CON MMSE	CON UPDRS III	DLB MMSE	DLB UPDRS III	PDD MMSE	PDD UPDRS III	PD MMSE	PD UPDRS III
AD			*	—	*	—	NS	—	NS	—	*	—
MCI	*	NS			*	—	*	—	*	—	†	—
CON	*	NS	*	NS			*	—	*	—	‡	—
DLB	NS	*	*	*	*	*			NS	‡	*	NS
PDD	NS	*	*	*	*	*	**NS**	**NS**			*	†
PD	*	*	NS	*	*	*	*	‡	*	NS		
	PC_{cog}	PC_{mot}	PC_{cog}	PC_{mot}	PC_{cog}	PC_{mot}	PC_{cog}	PC_{mot}	PC_{cog}	PC_{mot}	PC_{cog}	PC_{mot}

Post hoc tests (based on Wilcoxon tests) calculated separately on the 2 clinical scores, MMSE and UPDRS III (top-right/gray), and the 2 features, PC_{cog} and PC_{mot} (bottom-left/white), between all groups. Comparison between PDD and DLB (bold) is the only combination that showed insufficient group differences in both topological feature dimensions. Range of P values is indicated by the following: †$P < 0.05$; ‡$P < 0.01$; *$P < 0.001$.
— = clinical score not available; NS = no significant difference.
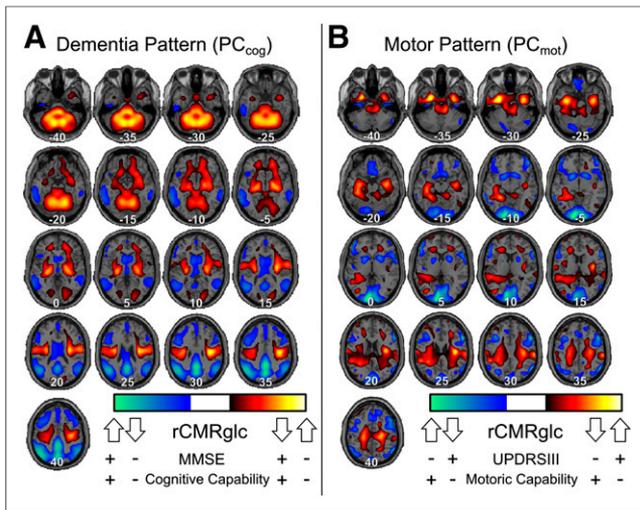
FIGURE 4. Visualization of principal patterns PC_{cog} and PC_{mot}. (A) Pattern related to PC_{cog} demonstrating high negative correlation with dementia score (MMSE). (B) Pattern related to PC_{mot} demonstrating high positive correlation with motor score (UPDRS III). Blue/cyan are regions in which rCMRglc measurements positively correlated with cognitive (A) or motor (B) capabilities, whereas red/yellow are regions in which these capabilities were negatively coupled with rCMRglc.

The SPM group comparisons showed the typical and well-described metabolic characteristics (Fig. 1; Supplemental Fig. 1) of each group (14). Only PDD and DLB showed no significant differences in the SPM metabolic group comparison. These 2 groups have PC_{cog} and PC_{mot} features with a strong overlap. Interestingly, clinical scores (MMSE and UPDRS III) in patients with PDD and DLB were also similar. Taken together, the overlap in clinical scores, metabolic group comparisons, and similarities in both measures of our PC analysis further questions the artificial separation of PDD and DLB. DLB and PDD most probably represent overlapping neurodegenerative disorders with a similar pathophysiology and pattern of metabolic changes, rather than distinctly different syndromes.

To validate and analyze our results in some more detail, we start our discussion by looking at the 2 rCMRglc reference patterns. Our Alzheimer pattern showed the well-described hypometabolism within the posterior cingulate cortex and in temporoparietal cortical areas (14,23–26). Our Parkinson pattern showed frontal and parietooccipital hypometabolism (Figs. 1B and 4B) in accord with Teune et al. (14). In the literature, neuroimaging data in PD are heterogeneous, both concerning methodology and results (27). Increases (12) and decreases (27,28) of glucose uptake within the basal ganglia have been reported in PD. Cortical metabolic abnormalities were reported in frontotemporal and parietooccipital areas (12,14,29–32).

The original expression values derived from these patterns from all subjects were correlated (Fig. 2A). This correlation implies that the expression values and their generating metabolic patterns cannot provide direct functionally specific information (because they were influenced by both diseases, PD and AD). The Figures 2B and 2C show the distribution of the decorrelated metabolic expression values and the position of each disease group in relation to the respective cognitive PC_{cog} and motor PC_{mot} metabolic pattern. Decoupling of the expression values into PC_{cog} and PC_{mot} expressions, achieved by the whitening transform, provides clearly functionally separated expressions and corresponding metabolic patterns

(correlation plots in Fig. 3 and corresponding metabolic patterns in Fig. 4).

The location of the mean expression vectors for each group (Fig. 2B) showed the centers of the CON, aMCI, and AD groups on a straight pure dementia line parallel to the PC_{cog} axis. Increased PD-like patterns in the PD, PDD, and DLB groups were reflected in the topographic map by their location above this pure dementia line, showing higher PC_{mot} expression values. Of special interest were the mean locations of the PDD and DLB groups. Both groups were located close to each other, reflecting the similarity of their metabolic representations. Post hoc tests between these 2 groups showed no significant differences in PC_{cog} and PC_{mot} expression values. This finding in some sense contradicts the results presented in a discriminant analysis study (33) in which the DLB and PDD groups were clearly distinguishable by their ^{18}F-FDG PET measurements. The reason for this discrepancy may be a result of the low subject sample size (8 DLB patients and 4 PDD patients) in this previous study, which was discussed as a major limitation of the study.

The group means of the PC_{cog} and PC_{mot} features of both the DLB and the PDD group are located above the AD group, corresponding to their motor deficits. This position of the PDD group in relation to the AD group is in accordance with a previous study (34) finding metabolic similarities between PDD and AD patients but diverging rCMRglc reductions in the occipital cortex and visual association areas as represented in our motoric pattern PC_{mot} (Fig. 4B).

The locations of the group means in the coordinate system also demonstrates that both the AD and the PD pattern are represented in the metabolic measurements. These metabolic measurements are related to the severity of clinical symptoms as demonstrated by the correlation analysis (Table 2; Fig. 3). The existence of these strong correlations between metabolic and clinical measurements qualifies the estimated features (PC_{cog} and PC_{mot}) as clinically meaningful. These features can be useful in supporting software tools to improve clinical differential diagnosis of age-associated neuropsychiatric disorders—that is, memory decline and extrapyramidal motor disturbances.

The successful application of AD-related spatial patterns to PD and PDD patients has already been described (35). However, in our study, we used a voxel-based approach without predefined regions of interest and additionally included the UPDRS III scores to detect extrapyramidal motor-related patterns. We then applied a statistical method to disentangle the individual metabolic pattern into both a cognition- and a motor-related component showing similarities with previously reported motor and cognitive patterns in nondemented PD patients (36). A detailed comparison is provided in the supplemental materials (sections II and III; Supplemental Figs. 2A and 2B). However, both the clinical characteristics of our patient groups and the methods described here differ significantly from the studies summarized by Peng et al. (36).

The representation of the measurements in the metabolic topographic map showed a considerable overlap between the features of the different disease groups. This overlap was most probably caused by similarities at the metabolic level in these groups. In some cases, clinically misclassified patients may also have contributed to this overlap. Nevertheless, we think that our data argue against a strict diagnostic categorization of different neurodegenerative disorders. Rather, the calculated metabolic maps implicate that a continuum exists on the neurometabolic level in these aging-associated disorders. Patients may benefit from a personalized treatment of motor and cognitive symptoms tailored for the individual patient

instead of categoric treatment decisions. This may be difficult, because physicians are still trained to think in categories, and therapies were often designed for clearly defined categoric diagnosis. A methodologic approach as introduced in this study may provide objective information to guide personalized treatments and possibly improve the health-related quality of life for patients in the future.

Limitations of our study pertain to the lack of neuropathologic confirmation of the clinical diagnosis. A proportion of patients might therefore be misclassified with respect to a pathologically based classification (35). However, our ranking methods did not rely on the unambiguous assignments, and it was not the goal to provide such an assignment.

CONCLUSION

The metabolic measurements and derived motor (PC_{mot}) and cognitive (PC_{cog}) features add further neuroimaging support to the notion that there is a continuous spectrum of neurodegenerative disorders ranging from PD to AD. This metabolic topological map can furthermore aid in ranking and localizing elderly patients within the neurodegenerative spectrum. On an individual patient level, the map may help to facilitate clinical diagnosis and support pharmacologic treatment decisions. Furthermore, our findings indicate that PDD and DLB may in fact represent 1 overlapping disease entity, characterized by the presence of mixed neuropathology and only different by the time course/onset of the individual subpathologies.

DISCLOSURE

The costs of publication of this article were defrayed in part by the payment of page charges. Therefore, and solely to indicate this fact, this article is hereby marked "advertisement" in accordance with 18 USC section 1734. No potential conflict of interest relevant to this article was reported.

REFERENCES

1. Ballard C, Ziabreva I, Perry R, et al. Differences in neuropathologic characteristics across the Lewy body dementia spectrum. *Neurology.* 2006;67:1931–1934.
2. Ince PG, Perry EK, Morris CM. Dementia with Lewy bodies: a distinct non-Alzheimer dementia syndrome? *Brain Pathol.* 1998;8:299–324.
3. Perl DP, Olanow CW, Calne D. Alzheimer's disease and Parkinson's disease: distinct entities or extremes of a spectrum of neurodegeneration? *Ann Neurol.* 1998;44:S19–S31.
4. Galpern WR, Lang AE. Interface between tauopathies and synucleinopathies: a tale of two proteins. *Ann Neurol.* 2006;59:449–458.
5. Perry EK, Irving D, Kerwin JM, et al. Cholinergic transmitter and neurotrophic activities in Lewy body dementia: similarity to Parkinson's and distinction from Alzheimer disease. *Alzheimer Dis Assoc Disord.* 1993;7:69–79.
6. Moussaud S, Jones DR, Moussaud-Lamodière EL, Delenclos M, Ross OA, McLean PJ. Alpha-synuclein and tau: teammates in neurodegeneration? *Mol Neurodegener.* 2014;9:43.
7. Irwin DJ, Lee VM-Y, Trojanowski JQ. Parkinson's disease dementia: convergence of α-synuclein, tau and amyloid-β pathologies. *Nat Rev Neurosci.* 2013;14:626–636.
8. Bertens D, Knol DL, Scheltens P, Visser PJ. Temporal evolution of biomarkers and cognitive markers in the asymptomatic, MCI, and dementia stage of Alzheimer's disease. *Alzheimers Dement.* 2015;11:511–522.
9. Lundström SL, Yang H, Lyutvinskiy Y, et al. Blood plasma IgG Fc glycans are significantly altered in Alzheimer's disease and progressive mild cognitive impairment. *J Alzheimers Dis.* 2014;38:567–579.
10. Emre M, Aarsland D, Brown R, et al. Clinical diagnostic criteria for dementia associated with Parkinson's disease. *Mov Disord.* 2007;22:1689–1707.
11. Herholz K. FDG PET and differential diagnosis of dementia. *Alzheimer Dis Assoc Disord.* 1995;9:6–16.
12. Eidelberg D, Moeller JR, Dhawan V, et al. The metabolic topography of parkinsonism. *J Cereb Blood Flow Metab.* 1994;14:783–801.
13. Ma Y, Tang C, Spetsieris PG, Dhawan V, Eidelberg D. Abnormal metabolic network activity in Parkinson's disease: test-retest reproducibility. *J Cereb Blood Flow Metab.* 2007;27:597–605.
14. Teune LK, Bartels AL, de Jong BM, et al. Typical cerebral metabolic patterns in neurodegenerative brain diseases. *Mov Disord.* 2010;25:2395–2404.
15. McKhann G, Drachman D, Folstein M, Katzman R, Price D, Stadlan EM. Clinical diagnosis of Alzheimer's disease: report of the NINCDS-ADRDA Work Group under the auspices of Department of Health and Human Services Task Force on Alzheimer's Disease. *Neurology.* 1984;34:939–944.
16. Hughes AJ, Daniel SE, Kilford L, Lees AJ. Accuracy of clinical diagnosis of idiopathic Parkinson's disease: a clinico-pathological study of 100 cases. *J Neurol Neurosurg Psychiatry.* 1992;55:181–184.
17. Fahn S. Assessment of the primary dystonias. In: Munsat T, ed. *The Quantification of Neurologic Deficit.* Oxford, U.K.: Butterworths; 1989:241–270.
18. McKeith IG. Consensus guidelines for the clinical and pathologic diagnosis of dementia with Lewy bodies (DLB): report of the Consortium on DLB International Workshop. *J Alzheimers Dis.* 2006;9:417–423.
19. Winblad B, Palmer K, Kivipelto M, et al. Mild cognitive impairment: beyond controversies, towards a consensus: report of the International Working Group on Mild Cognitive Impairment. *J Intern Med.* 2004;256:240–246.
20. Berres M, Monsch AU, Bernasconi F, Thalmann B, Stähelin HB. Normal ranges of neuropsychological tests for the diagnosis of Alzheimer's disease. *Stud Health Technol Inform.* 2000;77:195–199.
21. Soriano-Mas C, Pujol J, Alonso P, et al. Identifying patients with obsessive-compulsive disorder using whole-brain anatomy. *Neuroimage.* 2007;35:1028–1037.
22. Worsley KJ, Poline JB, Vandal AC, Friston KJ. Tests for distributed, nonfocal brain activations. *Neuroimage.* 1995;2:183–194.
23. Donnemiller E, Heilmann J, Wenning GK, et al. Brain perfusion scintigraphy with 99mTc-HMPAO or 99mTc-ECD and 123I-beta-CIT single-photon emission tomography in dementia of the Alzheimer-type and diffuse Lewy body disease. *Eur J Nucl Med.* 1997;24:320–325.
24. Herholz K, Salmon E, Perani D, et al. Discrimination between Alzheimer dementia and controls by automated analysis of multicenter FDG PET. *Neuroimage.* 2002;17:302–316.
25. Meltzer CC, Zubieta JK, Brandt J, Tune LE, Mayberg HS, Frost JJ. Regional hypometabolism in Alzheimer's disease as measured by positron emission tomography after correction for effects of partial volume averaging. *Neurology.* 1996;47:454–461.
26. Tam CWC, Burton EJ, McKeith IG, Burn DJ, O'Brien JT. Temporal lobe atrophy on MRI in Parkinson disease with dementia: a comparison with Alzheimer disease and dementia with Lewy bodies. *Neurology.* 2005;64:861–865.
27. Berding G, Odin P, Brooks DJ, et al. Resting regional cerebral glucose metabolism in advanced Parkinson's disease studied in the off and on conditions with [18F]FDG-PET. *Mov Disord.* 2001;16:1014–1022.
28. Antonini A, Vontobel P, Psylla M, et al. Complementary positron emission tomographic studies of the striatal dopaminergic system in Parkinson's disease. *Arch Neurol.* 1995;52:1183–1190.
29. Antonini A, De Notaris R, Benti R, De Gaspari D, Pezzoli G. Perfusion ECD/SPECT in the characterization of cognitive deficits in Parkinson's disease. *Neurol Sci.* 2001;22:45–46.
30. Firbank MJ, Colloby SJ, Burn DJ, McKeith IG, O'Brien JT. Regional cerebral blood flow in Parkinson's disease with and without dementia. *Neuroimage.* 2003;20:1309–1319.
31. Kuhl DE, Metter EJ, Riege WH, Markham CH. Patterns of cerebral glucose utilization in Parkinson's disease and Huntington's disease. *Ann Neurol.* 1984;15(suppl):S119–S125.
32. Piert M, Koeppe RA, Giordani B, Minoshima S, Kuhl DE. Determination of regional rate constants from dynamic FDG-PET studies in Parkinson's disease. *J Nucl Med.* 1996;37:1115–1122.
33. Garibotto V, Montandon ML, Viaud CT, et al. Regions of interest-based discriminant analysis of DaTSCAN SPECT and FDG-PET for the classification of dementia. *Clin Nucl Med.* 2013;38:e112–e117.
34. Vander Borght T, Minoshima S, Giordani B, et al. Cerebral metabolic differences in Parkinson's and Alzheimer's diseases matched for dementia severity. *J Nucl Med.* 1997;38:797–802.
35. Weintraub D, Dietz N, Duda JE, et al. Alzheimer's disease pattern of brain atrophy predicts cognitive decline in Parkinson's disease. *Brain.* 2012;135:170–180.
36. Peng S, Eidelberg D, Ma Y. Brain network markers of abnormal cerebral glucose metabolism and blood flow in Parkinson's disease. *Neurosci Bull.* 2014;30:823–837.